Measurement of Three-Dimensional Magnetic Properties With Feedback Control and Harmonic Compensation

Changgeng Zhang, Yongjian Li, *Member, IEEE*, Jingsong Li, Qingxin Yang, and Jianguo Zhu, *Senior Member, IEEE*

***Abstract*—Three-dimensional (3-D) magnetic fluxes exist in rotating electric machines and T-joints of three-phase power transformers, and may cause local overheating in these devices. In this paper, 3-D magnetic properties of the core materials are measured by an improved 3-D magnetic property tester. First, the 3-D magnetization system is modeled by the voltage and flux linkage equations. Their parameters including the self and mutual inductances and nonlinear impedance are analyzed by the finite element analysis and measured by experiments. Second, a magnetic feedback method in the frequency domain is proposed to obtain the desired magnetization loci. Third, when the specimen is in deep magnetic saturation, the harmonics of magnetic flux density waveform would affect the shape of the corresponding magnetic field strength loci and the accuracy of loss computation. Thus, a waveform compensation method is proposed to eliminate the effects of harmonics. Fourth, the tensor effects of H coils are eliminated by averaging the results of clockwise and counterclockwise rotational experiments. Finally, the 3-D magnetic test system with feedback control, harmonics compensation, and automated data processing is developed. By using the 3-D magnetic tester, samples of nonoriented silicon sheet steel are measured with various excitation models and the results are more reliable than those obtained by experiments without feedback and harmonics compensation.**

***Index Terms*—Electrical sheet steel, measurement of magnetic properties, rotational core losses.**

Manuscript received December 31, 2015; revised April 14, 2016; accepted April 19, 2016. Date of publication August 2, 2016; date of current version February 9, 2017. This work was supported in part by the National Natural Science Foundation of China under Grant 51237005, in part by the National Key Basic Research Program of China (973 Project) under Grant 2015CB251000, in part by the University Innovation Team Leader Program of Hebei Province under Grant LJRC003, and in part by the State Key Laboratory of Alternate Electrical Power Systems with Renewable Energy Sources under Grant LAPS16002.

C. Zhang, Y. Li, and J. Li are with the Province-Ministry Joint Key Laboratory of Electromagnetic Field and Electrical Apparatus Reliability, Hebei University of Technology, Tianjin 300130, China (e-mail: chang_geng@sina.com; liyongjian@hebut.edu.cn; 13702070369@163.com).

Q. Yang is with the Tianjin Key Laboratory of Advanced Electrical Engineering and Energy Technology, Tianjin Polytechnic University, Tianjin 300387, China (e-mail: qxyang@tjpu.edu.cn).

J. Zhu is with the School of Electrical, Mechanical and Mechatronic Systems, University of Technology Sydney, Sydney, NSW 2007, Australia (e-mail: Jianguo.Zhu@uts.edu.au).

Color versions of one or more of the figures in this paper are available online at http://ieeexplore.ieee.org.

Digital Object Identifier 10.1109/TIE.2016.2597118

I. Introduction

SILICON sheet steels are widely employed as the materials of magnetic cores in various electromagnetic devices, such as power transformers, rotating electrical machines, and electromagnets. The magnetic properties of silicon sheet steels are key factors in design and performance optimization of these electromagnetic devices [1]. The accuracy of core loss computation in rotating electrical machines can be improved by considering the rotational magnetic properties, which can be measured by two-dimensional (2-D) magnetic property testing methods [2]. In 2-D methods, single sheet specimens of various shapes are adopted, such as square, hexagonal, and circular specimens [3]–[5]. The magnetic excitation circuits of these 2-D testers are mainly either horizontal or vertical cross structures [6]. In most power transformers and motors, the desired magnetic flux path is confined within the plane of electrical steel sheets. In reality, however, many factors such as the burred region in the core, butt and lap, and mitred overlap corner configurations in a transformer would produce magnetic fluxes crossing the laminated steel sheets, which is a three-dimensional (3-D) electromagnetic problem [7]. In this situation, extra core losses are generated [8]. The classical eddy losses in three orthogonal directions can be computed either analytically by solving the Maxwell equations in differential form [9] or numerically by using the finite element method (FEM) [10]. The vectorial magnetic hysteresis loss, on the other hand, is much more complicated. The traditional solution is only the superposition of scalar magnetic models in three directions, which relies on the results of one-dimensional (1-D) magnetic testing. An engineering problem related to the 3-D magnetic flux is the magnetic shielding steel plates on the oil tank of large power transformers, which is established in the testing electromagnetic analysis method (TEAM) Workshop Problem 21 [11]. The difficult part of the problem is that the magnetic properties in the plane of laminated silicon steels are also influenced by the magnetic field in the laminated direction [12]. Thus, it is essential to measure the 3-D magnetic properties for the 3-D magnetic modeling to enable design optimization of the shielding structure in TEAM problem 21 and reduce the 3-D stray field losses of power transformers [13].

In the magnetic properties measurement, the standard excitation model is to control the locus of either magnetic flux density ($\boldsymbol{B}$) or magnetic field strength ($\boldsymbol{H}$). The classical

0278-0046 © 2016 IEEE. Personal use is permitted, but republication/redistribution requires IEEE permission.
See http://www.ieee.org/publications_standards/publications/rights/index.html for more information.

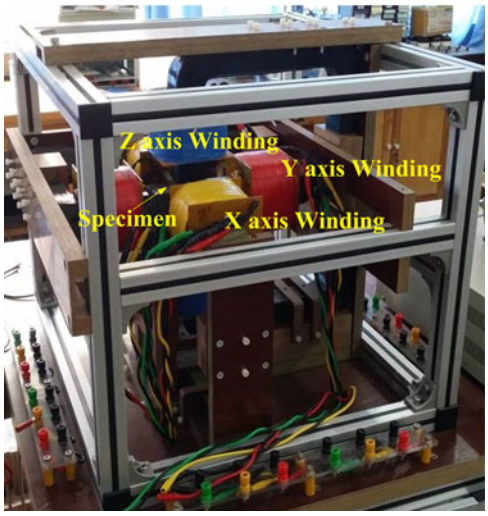


Fig. 1. Photograph of the 3-D magnetization structure with "C-type" cores.

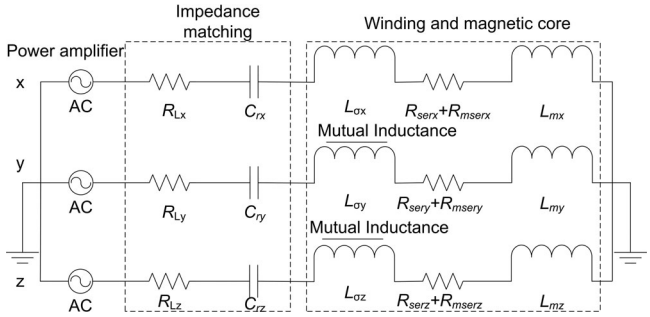


Fig. 2. Equivalent circuit of the 3-D magnetic tester.

feedback control method with PI regulator works well in the linear region of magnetization property. However, it can be very difficult to achieve the desired magnetization loci in a material with strong anisotropy in 2-D or 3-D magnetic measurement. In the nonlinear control of dc or induction motor, the magnetic flux can be observed by nonlinear scalar magnetic saturation model [14], [15]. While in the control of 3-D magnetic tester, B and H can be directly measured by the combined $B-H$ sensing coils. The nonlinear flux is highly affected by the 3-D magnetic saturation and hysteresis model [16].

An adaptive digital feedback method for 1-D and 2-D magnetic measurements was designed with multivariable inputs and outputs [17]. The digital control of the flux loci based on contraction mapping principle has good performance on the three-phase single sheet tester [18], [19]. For 3-D magnetic testing, however, the specimen is a cube made of 70–80 silicon steel sheets unlike the one single sheet specimen in 1-D and 2-D measurements so that the excitation power needs to be increased significantly. Thus, the excitation circuit is more complex and the traditional control method cannot be directly extended to the 3-D magnetic properties measurement.

In this paper, a 3-D magnetic properties measurement apparatus is designed. A novel feedback control method in the frequency domain is proposed and implemented by a digital controller. Furthermore, the harmonics induced by the 3-D magnetic saturation are effectively suppressed by a waveform compensation algorithm. The 3-D magnetic properties of the silicon sheet steel (35WW270) are measured by the 3-D magnetic tester using the novel control method.

II. Modeling of the 3-D Magnetic Testing System

A. Improved 3-D Magnetization Structure

Fig. 1 shows the improved 3-D magnetization structure consisting of three orthogonal C-cores and six multilayer excitation windings wound around the corresponding orthogonal magnetic poles [13]. Each C-core is one piece cut from a wounded square-shaped core with highly grain-oriented laminated silicon steel (27ZH95). In the 3-D magnetization system, a cubic specimen made of 80 layers of silicon steel sheets is placed in the center of the 3-D tester, and the side length of magnetic core is 0.7 m. Because of significantly larger sizes of the specimen and tester yokes than those of the 1-D and 2-D magnetization systems, much higher magnetomotive force is required to saturate the specimen, and this makes the 3-D flux density waveform control extremely difficult.

B. Analysis of the 3-D Excitation Model

The 3-D magnetic testing system consists of three channels of power amplifier, matching impedance, compensation capacitor, and excitation windings. The equivalent circuit of the 3-D tester is illustrated in Fig. 2. In order to analyze the 3-D rotational excitation feature, the transient voltage equations of the equivalent circuit can be written as

$$\begin{cases} \boldsymbol{u} = R_L \boldsymbol{i} + \boldsymbol{C}_r{}^{-1} \int \boldsymbol{i} dt + R_w \boldsymbol{i} + \frac{d\boldsymbol{\lambda}}{dt} \\ \boldsymbol{u}_m = \boldsymbol{R}_{\mathrm{xyz}} \frac{d\boldsymbol{\lambda}_m}{dt} \end{cases} \tag{1}$$

where $\boldsymbol{u}$ and $\boldsymbol{i}$ denote the 3-D voltage and current space vectors of the power amplifier, R_L is the compensation resistance of impedance matching, R_w the diagonal matrix of the excitation winding resistance, C_r the diagonal matrix of the resonant capacitance, λ and $\boldsymbol{\lambda}_m$ the flux linkage space vectors through the main magnetic circuit and the specimen, respectively.

Since the cubic specimen cannot be perfectly located in the center of three exciting magnetic poles, a space rotating matrix of the specimen in the coordinate system of the 3-D magnetic poles, $\boldsymbol{R}_{\mathrm{xyz}}$, is employed, and it can be determined by

$$\boldsymbol{R}_{\mathrm{xyz}} = \boldsymbol{R}_{\mathrm{xy}} \boldsymbol{R}_{\mathrm{xz}} \boldsymbol{R}_{\mathrm{yz}} \tag{2}$$

where $\boldsymbol{R}_{\mathrm{xy}}, \boldsymbol{R}_{\mathrm{xz}}$, and $\boldsymbol{R}_{\mathrm{yz}}$ are the rotating transform matrices in the *xoy, xoz*, and *yoz* planes, respectively. They can be

expressed as

$$\boldsymbol{R}_{\mathrm{xy}} = \begin{bmatrix} \cos(\theta_{\mathrm{xy}}) & -\sin(\theta_{\mathrm{xy}}) & 0 \\ \sin(\theta_{\mathrm{xy}}) & \cos(\theta_{\mathrm{xy}}) & 0 \\ 0 & 0 & 0 \end{bmatrix}$$

$$\boldsymbol{R}_{\mathrm{xz}} = \begin{bmatrix} \cos(\theta_{\mathrm{xz}}) & 0 & -\sin(\theta_{\mathrm{xz}}) \\ 0 & 0 & 0 \\ \sin(\theta_{\mathrm{xz}}) & 0 & \cos(\theta_{\mathrm{xz}}) \end{bmatrix}$$

$$\boldsymbol{R}_{\mathrm{yz}} = \begin{bmatrix} 0 & 0 & 0 \\ 0 & \cos(\theta_{\mathrm{yz}}) & -\sin(\theta_{\mathrm{yz}}) \\ 0 & \sin(\theta_{\mathrm{yz}}) & \cos(\theta_{\mathrm{yz}}) \end{bmatrix}$$

where θ_{xy}, θ_{xz}, and θ_{yz} are the rotational angles of the specimen in the *xoy*, *xoz,* and *yoz* planes, respectively. The main flux is defined as the magnetic flux crossing the specimen. The flux linkage equations can be expressed as

$$\begin{cases} \boldsymbol{\lambda} = L_\sigma \boldsymbol{i} + L_m \boldsymbol{i} + (R_{\mathrm{ser}} + R_{\mathrm{mser}}) \int_0^t \boldsymbol{i} dt \\ \boldsymbol{\lambda}_m = (L_m \boldsymbol{i} + R_{\mathrm{mser}} \int_0^t \boldsymbol{i} dt) \end{cases} \tag{3}$$

where $\boldsymbol{L}_m$ and L_σ are the excitation and leakage inductances of the excitation windings, which highly depends on the magnetic properties of specimen. For a specimen of magnetically isotropic material, e.g., soft magnetic composite (SMC) material, $\boldsymbol{L}_m$ is a diagonal matrix. While for specimens of grain-oriented and nonoriented silicon sheet steels and magnetically anisotropic materials, $\boldsymbol{L}_m$ has nonzero off-diagonal elements. $\boldsymbol{R}_{\mathrm{ser}}$ and $\boldsymbol{R}_{\mathrm{mser}}$ are the series equivalent resistors diagonal matrix of hysteresis losses in the main magnetic circuit and specimen.

C. Simulation and Experiment for Model Parameter

In magnetic testing, the cubic specimen with sensing coils placed in the center of three orthogonal magnetic poles should be magnetized by a strong and homogeneous magnetic field. Between the poles and specimen, however, the surface sensing coils must form air gaps. This can cause the magnetizing field far away from uniformity. To reduce this influence, six thin guard pieces with the same material and same lamination direction are fabricated and placed around the cubic specimen. The 1 mm air gap around the specimen is used for placing the B and H sensing coils as shown in Fig. 3. The circular B and square H sensing coils are all induction coils attached to the surface of the specimen [10], [13]. Before the experiments, the 3-D magnetization structure is modeled and analyzed by FEM with software ANSYS Maxwell. The effectiveness of using guard pieces is explicitly proven by the FEM simulation results that the $\boldsymbol{B}$ and $\boldsymbol{H}$ fields are inhomogenous on the surfaces of guard pieces but homogenous in the center of specimen surfaces, where the sensing coils are attached.

In order to change the specimen for ease of control, each magnetic core is cut into two parts so that the air gaps are inevitable. Consequently, the relatively lower inductance and more complex leakage flux of the 3-D tester are obvious, compared with

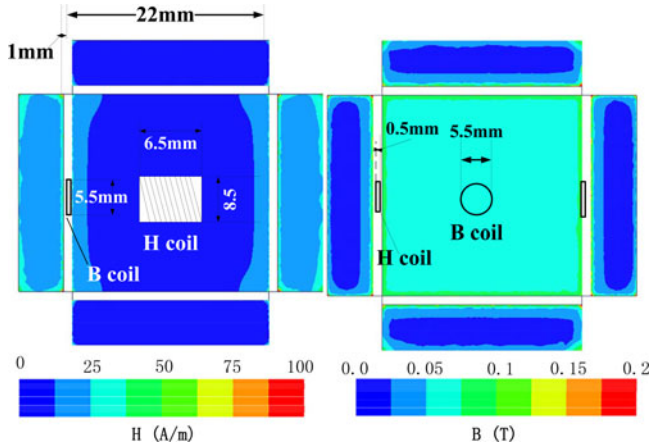


Fig. 3. *B–H* sensing coils, *B* and *H* distribution of the specimen.

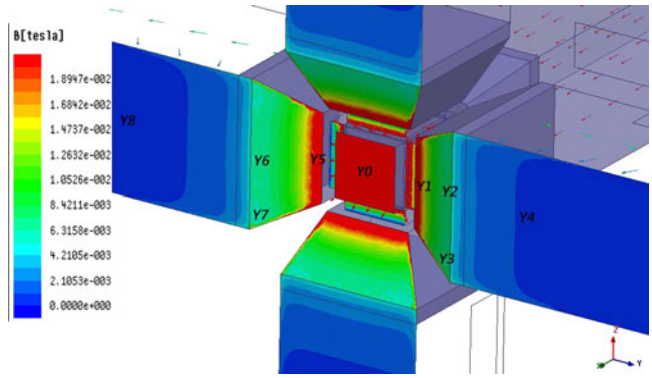


Fig. 4. Magnetic flux density distribution of the specimen surface and leakage flux distributions of the vicinity core poles and air gaps.

the traditional power transformers. Fig. 4 illustrates the simulation results of magnetic field distribution when only the *x*-axis of the 3-D tester is excited. In the plot, one part of the core pole is removed in order to clearly illustrate the magnetic field distribution on the specimen surface and the leakage flux distributions at the vicinity of core poles and air gaps. As shown, the $\boldsymbol{B}$ distribuation on the specimen surfaces is homogenous, and thus the measurement precision is guaranteed. In order to verify the validity of simulation, the experimental setup is built. The B and H signals of the specimen are recorded by NI$^{\mathrm{TM}}$ DAQmx PXIe-6368. The synchronizing voltage and current of the excitation windings are monitored by Zimmer$^{\mathrm{TM}}$ Power Analyzer, and the space magnetic field is measured by Lakeshore$^{\mathrm{TM}}$ 3D Gauss Meter. Table I compares the simulation and experimental results at the denoted points in Fig. 4 . Most of the simulation results on the surface of the specimen and magnetic poles match well with the experimental results. However, the magnetic flux density at the corner of the magnetic pole, denoted by Y3 and Y7, changes sharply. This may be attributed to the experimental error due to the fact that a small displacement of the Gauss meter hall probe may cause a relatively big error.

Fig. 5 shows the proportion of flux linkage to the flux around the specimen, where the flux linkage due to the magnetizing

TABLE I
COMPARISON BETWEEN THE SIMULATED AND EXPERIMENTAL MAGNETIC FLUX DENSITY AT THE MEASUREMENT POINTS

Point	$B_{\rm sim}$ (Gs)	$B_{\rm exp}$ (Gs)	Point	$B_{\rm sim}$ (Gs)	$B_{\rm exp}$ (Gs)
Y0	730	678	Y5	95.56	120
Y1	100.64	109	Y6	46.70	52.5
Y2	45.907	46.7	Y7	115.64	57.4
Y3	116.62	58	Y8	14.40	17.3
Y4	14.45	16.1			

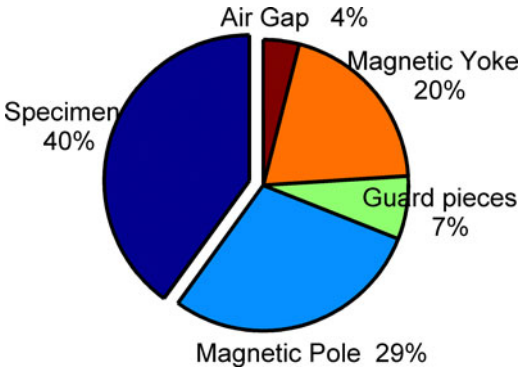


Fig. 5. Proportion of excitation winding flux linkage to the flux around the specimen.

flux through the specimen, denoted as $\boldsymbol{\lambda}_m$ in (1), only accounts for 40% of the main magnetic flux linkage, denoted as λ in (1). Although the value of $\boldsymbol{B}$ on the surface of magnetic poles and yokes is very small, the area is much larger than that of the specimen so that their flux linkage can be significant. As a result, the $\boldsymbol{L}_m$ and L_σ in (3) can be computed by the electromagnetic simulation as presented above. Also, these system parameters can be identified by rotational magnetization experiments when the specimen is under rotational magnetizations in the *xoy* plane, such as the mutual inductance coefficient between the *x*- and *y*-axes, leakage inductance, series equivalent resistance, and impedance of the excitation system, as shown in Fig. 6.

Based on the measurement results with the excitation current from 0 to 6 A, the parameters in (1) and (3) can be identified. As the excitation current increases, the magnetic core and specimen are magnetized close to saturation, and $L_m + L_\sigma$ and $R_{\rm mser} + {\rm R}_{\rm ser}$ will decrease. The increasing rate of the magnetic core loss will decrease. Moreover, the magnetic poles on the *x*-, *y*-, and *z*-axes in the simulation model are exactly vertical with each other, and consequently the mutual inductance between different windings should be zero. However, practical asymmetry and assembling error of the magnetic cores would cause noticeable nonlinear mutual inductances between these windings.

III. CONTROL METHOD FOR 3-D TESTING SYSTEM

In order to achieve the desired magnetization and reliable testing signals for a given specimen, an electromagnetic feedback control method is designed and applied in the 3-D magnetic property measurement. The precision and repeatability of the measurement depend strongly on the control method, which is associated with the corresponding excitation model.

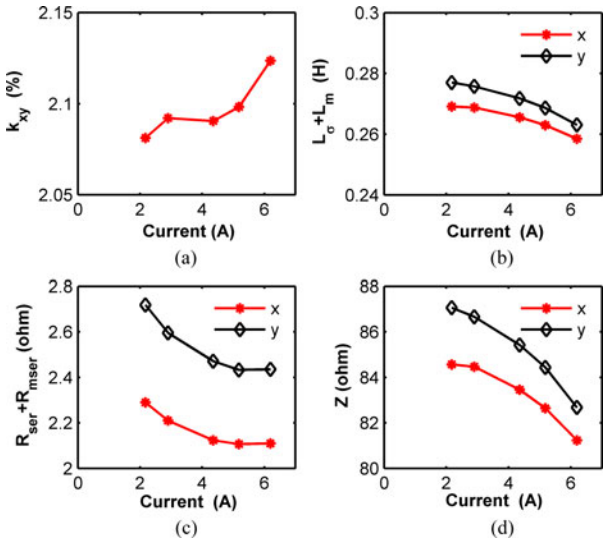


Fig. 6. Parameter identification versus excitation current at 50 Hz: (a) Mutual inductance coefficient between *x*- and *y*-axes, (b) leakage inductance, (c) series equivalent resistance, and (d) excitation impedance.

A. Excitation Models

1) 2-D Rotating Excitation Model: So far, there is no industrial standard for 2-D magnetic property testing. The most widely used 2-D rotating excitation model is circular or elliptic magnetization in a plane, which can be expressed as

$$\begin{cases} B_x(t) = B_m \cos(2\pi f t) \\ B_y(t) = \varepsilon_y B_m \cos(2\pi f t + \pi/2) \end{cases} \tag{4}$$

where f is the excitation frequency, $\boldsymbol{B}_m$ the magnitude of rotating flux density vector $\boldsymbol{B}$, and ε_y the ratio of the major and minor axes. According to Faraday's law of electromagnetic induction, the derivate of (4) versus time is proportional to the back EMF of the winding, and is used as the feedback signal in the feedback system.

On one hand, the mutual inductance between the *x*- and *y*-axes exists due to the misalignment of the two opposite magnetic poles. On the other hand, the magnetic circuit parameters along the *x*- and *y*-axes are not identical to each other. The open-loop control method fails to satisfy the phases and magnitudes of the two directional waveforms and the resultant $\boldsymbol{B}$ locus is a distorted circular or elliptic one.

2) Spherical Excitation Model: The conventional magnetization techniques examine the overall hysteresis under 1-D and 2-D excitations, which cannot obtain experimetal data in the direction perpendicular to the lamination plane. In fact, the nature of the magnetization process suggests that the magnetic properties should be studied under 3-D excitations. By setting the associated trigonometric equations in three

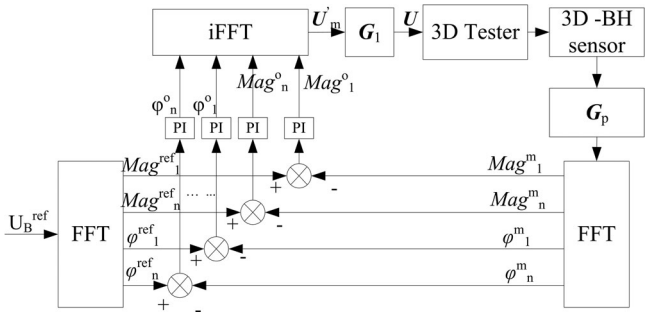


Fig. 7. Control flow chart of 3-D magnetic testing in frequency domain.

directions, a $\boldsymbol{B}$ vector spiral spherical model is established as the following:

$$\begin{cases} B_x(t) = B_m \cos(2\pi f_1 t)\cos(2\pi f_2 t) \\ B_y(t) = \varepsilon_y B_m \sin(2\pi f_1 t)\cos(2\pi f_2 t) \\ B_z(t) = \varepsilon_z B_m \sin(2\pi f_2 t) \end{cases} \tag{5}$$

where ε_z is the ratio of the $\boldsymbol{B}$ magnitudes in the z- and x-axes, and ε_y the ratio of the $\boldsymbol{B}$ magnitudes in the y- and x-axes. The frequency f_2 is set very low to suppress the eddy current parallel to the plane of silicon steel sheets. If the eddy current in the plane of silicon steel sheets is significant, the magnetic field is extremely inhomogeneous and the measurement results will be unreliable. The envelope of the $\boldsymbol{B}_x$ and $\boldsymbol{B}_y$ waveforms is a sinusoidal waveform of frequency f_2. Unlike the 1-D and 2-D excitation model, the 3-D spiral spherical excitation model is involved in two different frequencies in one exciting axis.

B. Feedback Control Method

1) Frequency Domain Control Method in Magnetic Measurement: In magnetic property measurement, the feedback control method can be in either time domain or frequency domain. The classical time domain algorithm can control the transient magnetization process with quick response, but its digital realization needs high speed computation resources. In general, the ac magnetic properties of soft magnetic materials are measured under a steady and periodic magnetization excitation. Therefore, the signal frequency spectrum analysis and frequency domain control can be more effective. Actually, the feedback control method in 3-D testing is focused on the nonlinear multi-input and multioutput control problem.

In the control flow chart shown in Fig. 7, φ_k^{ref} and $\mathrm{Mag}_{\mathrm{k}}^{\mathrm{ref}}$ are the reference phase and magnitude of EMF for a specified $\boldsymbol{B}$, respectively, and k is the order of harmonics. The EMFs of the 3-D vector $\boldsymbol{B}$ measured by the 3-D-*BH* sensor are processed by the amplifier and filter circuit as denoted G_{p}. Similarly, the phase φ_k^m and magnitude $\mathrm{Mag}_{\mathrm{k}}^{\mathrm{m}}$ are transformed by FFT from the processed EMF-$\boldsymbol{B}$ signals. Thus, the phase and magnitude are independently controlled by the classical PI feedback method at all different frequencies by

$$\begin{aligned} \mathrm{Mag}_k^o &= K_p^{\mathrm{mag}}(\mathrm{Mag}_k^{\mathrm{ref}} - \mathrm{Mag}_k^m) \\ &\quad + K_I^{\mathrm{mag}} \int (\mathrm{Mag}_k^{\mathrm{ref}} - \mathrm{Mag}_k^m)dt, \\ \varphi_k^o &= K_p^{\varphi}(\varphi_k^{\mathrm{ref}} - \varphi_k^m) + K_I^{\varphi} \int (\varphi_k^{\mathrm{ref}} - \varphi_k^m)dt \end{aligned} \tag{6}$$

where K_p^{mag} and K_p^{φ} are the proportional gain, and K_I^{mag} and K_I^{φ} the integral gain of the magnitude and phase, respectively.

After regulated by the PI controllers, all the phase angle $\varphi_1^o - \varphi_n^o$ and all the magnitude $\mathrm{Mag}_1^o - \mathrm{Mag}_n^o$ are combined by the Fourier series method into the waveform

$$U'_m = \sum_k \mathrm{Mag}_k^o \cos(2\pi f_k t + \varphi_k^o) \tag{7}$$

where f_k is the frequency of the kth harmonic. In Fig. 2, the impedance matching resistor and capacitor is composed of a low-pass filter circuit, which can regulate the phase angle in the magnetic circuit. Various adaptive digital feedback techniques were proposed to compensate the lagging phase angle according to the excitation frequency and magnetizing impedance [17]. In the proposed method, the excitation procedure is described by a transfer function $\boldsymbol{G}_1$, which is deduced from (1) and (3)

$$\begin{aligned} \boldsymbol{G_1} &= \frac{\boldsymbol{U}(s)}{\boldsymbol{U'_m}(s)} = [(\boldsymbol{R_L} + \boldsymbol{R_w} + \boldsymbol{R_{ser}}(s) + \boldsymbol{R_{mser}}(s)) \\ &\quad + \frac{\boldsymbol{C}_r^{-1}}{s} + (\boldsymbol{L}_\sigma + \boldsymbol{L}_m)s](s\boldsymbol{L}_m^{-1} + \boldsymbol{R}_{\mathrm{mser}}^{-1}(s)) \end{aligned} \tag{8}$$

where the given three-channel excitation signal U'_m needs to be amplified and compensated by series resonance, and U is the ultimate excitation voltage. The function of $\boldsymbol{G}_1$ can decouple the mutual inductances among the x, y, and z magnetizing axes.

The nonlinear relationship of vector hysteresis between $\boldsymbol{B}$ and $\boldsymbol{H}$ cannot be expressed in simple theory. Instead, the nonlinear problem is approximated as a piecewise linear problem. In the process of magnetic properties measurement, the compensation model computation depends on the magnitude of excitation current due to the nonlinear saturated inductance. The magnetic field signals of the magnetized specimen are measured by the 3-D-*BH* sensor. When the relative error between the measurement and reference (magnitudes and phases) is less than 0.3%, the measurement process is completed and the results are recorded automatically.

2) Digital PI Controller: Due to variable magnitude and frequency of vector flux density, the parameters of analog PI controller in magnetic measurement system are difficult to determine. Besides, random air gaps exist between the magnetic pole and specimen in the rotational magnetic property testing system. The main and leakage inductances will be changed in accordance. The digital controller can regulate the PI parameters automatically according to the difference of magnitude and frequency of $\boldsymbol{B}$. Thus, the digital control method in rotational magnetic measurement process will be more flexible and robust.

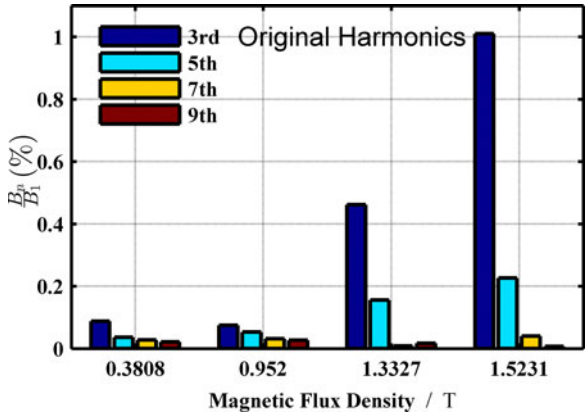


Fig. 8. Ratio of harmonics to fundamental components in the *x*-axis under rotational magnetic measurement without harmonic compensation.

In the magnetization process, hysteresis phenomenon can cause remanence and magnetic multivaluedness. The magnetization loci or hysteresis loops would be changed with a random magnetization start point. In this controller, the proportional gain K_p^{mag} should be set to an appropriate value. Otherwise, the output signal magnitude Mag*o k* will fluctuate at the referenced magnitude of *B*. Therefore, overshoot of the PI controller can be avoided, and reproducible experiment results can be achieved.

IV. Waveform Compensation of 3-D Magnetic Property Measurement

There will be slightly distortion in the $\boldsymbol{B}$ waveform when the specimen is magnetized to saturation, and the measured hysteresis loci and core losses would deviate from the normal values. A waveform compensation method is proposed for the 3-D magnetic property measurement.

A. Waveform Distortion Analysis

In order to concentrate the magnetic flux through the specimen, the magnetic pole is designed in quadrangular frustum shape. When the specimen is magnetized to saturation, the magnetic core works at the knee-point of *B*-*H* curve, where the nonlinear problem starts. Fig. 8 shows the ratio of $\boldsymbol{B}$ harmonics to the fundamental component in the *x*-axis when the specimen is magnetized with a rotating magnetic flux in the *xoy*-plane without waveform feedback. As the fundamental component of $\boldsymbol{B}$ is increasing close to the saturation state, the high-order harmonics of $\boldsymbol{B}$ is increasing more and more.

B. Theory of Waveform Compensation

The previous feedback control method focused on the waveform at the fundamental frequency but neglected the harmonics component caused by saturation. The phase and magnitude cannot be decoupled to control independently during the harmonic suppressing. Compared with the fundamental component feedback control method, in the proposed waveform compensation algorithm, the zero magnitude set point (SP) is concerned and the phase angle SP is neglected.

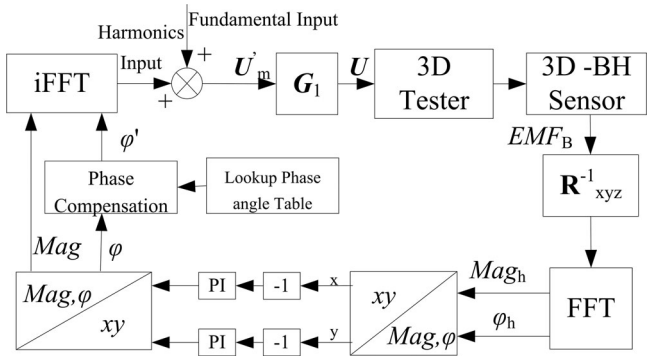


Fig. 9. Control flowchart of harmonic compensation algorithm.

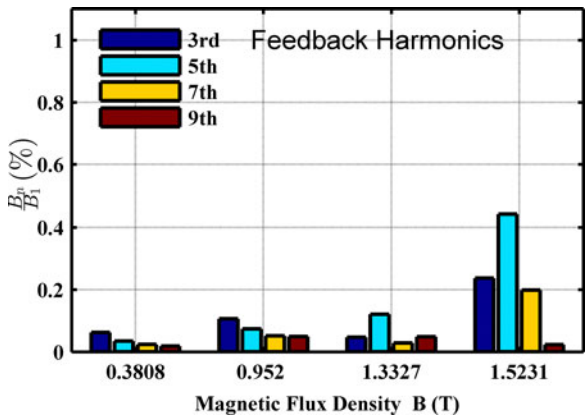


Fig. 10. Ratio of harmonics to fundamental components in the *x*-axis under rotational magnetization with harmonic compensation.

The basic principle of this method is to add the corresponding harmonics to compensate the distorted $\boldsymbol{B}$ waveform. Fig. 9 shows the control flowchart of the harmonic compensation algorithm. EMFs of $\boldsymbol{B}$ are measured by the 3-D-*BH* sensors and are transferred by inverse rotational matrix R_{xyz}. $\mathrm{Mag_h}$ and φ_h are the magnitudes and phases of the 3rd, 5th, and 7th harmonics, respectively. They are then transformed to process values in the 3rd, 5th, and 7th harmonic space by the transformation from the polar coordinates to the Cartesian coordinates. The next step is the PID control, where the SP vector in the harmonic space is set zero for harmonics suppressing. After that, the output variables are transformed from the Cartesian coordinates back to the polar coordinates. To handle the nonlinear phase response at different frequencies, a phase compensation is applied to the PID output signal φ, and the amount of phase compensation is obtained from a predefined look-up table of phase angles. The processed Mag and φ' are then transformed to the harmonic waveform input by the inverse FFT. The combined input waveform U'_m is decoupled in space by transformation G_1 and then fed to the 3-D magnetic tester.

Before the waveform compensation experiment, the lagging phase angles caused by the nonlinear power amplifier are measured to form a look-up table. The function of compensation phase angles is with respect to the excitation magnitude and frequency.

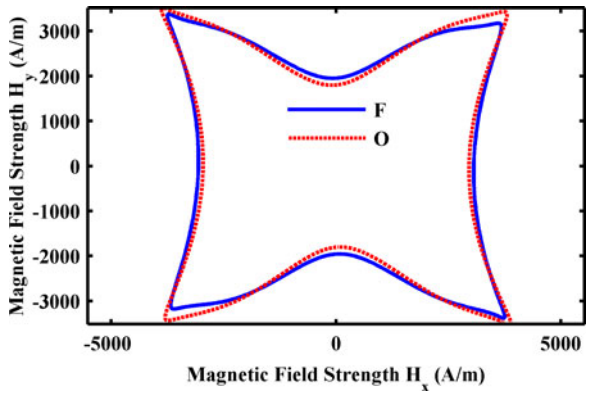


Fig. 11. Comparison of $\boldsymbol{H}$ loci under rotational magnetization between the feedback (F) compensation and the original (O) method.

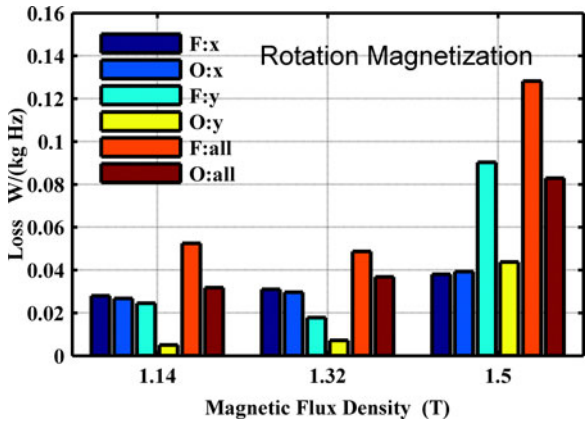


Fig. 12. Comparison of rotational magnetization loss of one loop between the feedback (F) and the original (O) method.

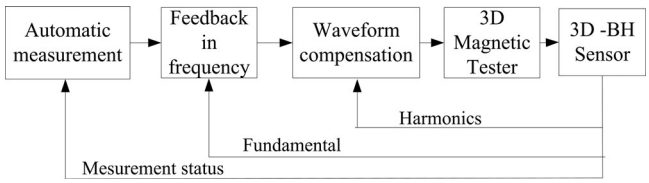


Fig. 13. Schematic diagram of the automated measurement system.

C. Verification of Harmonic Compensation for 3-D Magnetic Property Measurement

For nonoriented silicon sheet steel 35WW270, the rotational magnetic properties at 50 Hz are measured by the proposed harmonic compensation method. Compared with Fig. 8, Fig. 10 shows the ratios of harmonics to fundamental component in the x-axis under rotational magnetization with the harmonic compensation method. It can be noted that when the specimen is magnetized from the initial stage to saturation, the $\boldsymbol{B}$ harmonics measured with harmonic compensation are greatly reduced. While the third harmonic of waveform by the harmonic compensation method is reduced greatly compared to those obtained by the original frequency domain feedback experiment, the fifth and seventh harmonics increase slightly due to the nonlinear magnetization.

In the rotational magnetic property measurement with feedback control, the saturation effect only produces slight change of vectorial $\boldsymbol{B}$ in magnitude. However, any slight disturbance of $\boldsymbol{B}$ loci can cause significant changes of $\boldsymbol{H}$ loci, especially at 45°, as shown in Fig. 11. The sharpness of $\boldsymbol{H}$ loci, on the other hand, is weakened when the $\boldsymbol{B}$ harmonics are eliminated by waveform compensation. Besides, the x and y intercepts of the $\boldsymbol{H}$ loci become larger. The measured magnetic anisotropy of nonoriented silicon steel becomes weaker. By comparing the results before and after the waveform compensation, the maximum relative error of H_x waveforms is 4.4%, and the maximum relative error of H_y waveform is 7.5%. The rotational magnetization losses between the two methods are compared in Fig. 12. The losses in the x-axis between the two methods are similar, while the loss in the y-axis obtained by the feedback compensation method is larger than that by the original method. The total loss after the compensation is also larger than that before the compensation. As a result, the rotational magnetization measurement by waveform compensation can illustrate the magnetic anisotropy and loss properties more exactly.

V. 3-D Magnetic Property Measurement of Silicon Steel Laminations

Based on the magnetic property feedback and waveform compensation method, a series of experiments including 1-D alternating magnetization, 2-D rotating magnetization, and 3-D spherical magnetization are carried out for a sample of nonoriented silicon steel laminations in a broad range of frequencies (20 Hz–1 kHz).

TABLE II
Coefficients of B and H Coils

Coefficient (m^2)	x-axis	y-axis	z-axis
H coils	0.002556	0.002597	0.002627
B coils	0.002363	0.002363	0.002359

A. Automated Measurement System

The automated measurement system consists of three layers, as shown in Fig. 13. The inner layer is for waveform compensation. The medium layer is for feedback control in the frequency domain, and the outer layer is for automated processing. The function of the automated processing system includes measurement status monitoring, measurement queue setting, magnetization stability time delay, output recording, and online processing.

B. Tensor Coefficient of H Coils

The 3-D magnetic property sensing system consists of 3-D magnetic sensing coils, high-resolution signal conditioning circuit, and data acquisition system. The coefficients of the sensing coils are product of the area and number of turns, which is calibrated by the solenoid. The diagonal coefficients of the B and H coils are shown in Table II. The maximum relative permeability (μ_r) of high grain silicon steel is more than 10 000, so that

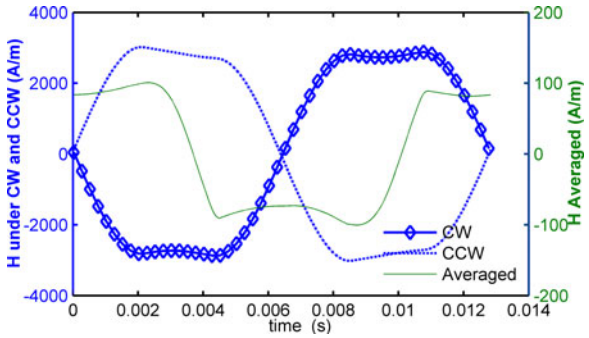


Fig. 14. EMF of *H* under CW and CCW rotation.

the induction signal of the H coil is very tinny, which needs to be amplified by 1000–100 000 times depending on the relative permeability.

However, the EMF of H sensing coil is not only inducted by $\boldsymbol{B}$ along the measuring direction but also along the transverse direction. For example, when the measured specimen is rotational magnetization, the EMF of $H_{\boldsymbol{x}}$ coil should be calculated by

$$\mathrm{EMF_{Hx}} = K_{\mathrm{hxx}}\mu_0 \frac{d\boldsymbol{H}_x}{dt} + K_{\mathrm{hxy}} \frac{d\boldsymbol{B}_y}{dt} \tag{9}$$

where K_{hxx} is the coil coefficient of the H_x coil and K_{hxy} the tensor coefficient of the B_y coil. The typical measured value of K_{hxy} is $3 \times 10^{-}5$ m^2 and affected by the flux density along the y direction. If $\boldsymbol{B}_x = \boldsymbol{B}_{\mathrm{y}} = \mu_0\mu_{\mathrm{r}}\boldsymbol{H}_{\mathrm{x}}$, the second part in (9) would be 100 times larger than that of the concerned first part. In order to solve this problem, one method is to exactly measure the tensor coefficient of H_x by alternating magnetization experiment in the x-, y-, and z-axes. Since the tensor coefficient of the B_y coil is very small and could be neglected, B_y can be directly measured. Then, H_x can be obtained by solving (9).

In order to investigate the tensor coefficient K_{hxy}, the tensor reluctivity ν_{xy} is defined when only the y-axis is excited as

$$\nu_{\mathrm{xy}} = \frac{H_x}{B_y} = \frac{K_{\mathrm{hxy}}}{K_{\mathrm{hxx}}\mu_0} \tag{10}$$

where ν_{xy} is not constant but depeding on the frequency and intrinsic magnetic properties of the specimen. As the excitation frequency increasing, the skin effect of the magnetic flux inside the specimen takes effects on the decreasing of ν_{xy}. Furthermore, for different magnetic material, K_{hxy} is a different mutivariable function with respect to f and $\boldsymbol{B}$.

The other method to eliminate the tensor coefficient influences is to measure the magnetic properies of specimen under clockwise (CW) and counterclockwise (CCW) magnetizations with the same excitation magnitude. When the measured B_y under CW and CCW are in the same magnitude and inverse direction, the desired part of $\mathrm{EMF_{Hy}}$ are identical but the tensor parts in (9) are opposite. Therefore, the tensor part can be eliminated by averaging the measured $\mathrm{EMF_{Hy}}$ in the CW and CCW directions. However, the difference of the measured EMF of H under CW and CCW rotation is less than 1%, as shown in Fig. 14. As a result, a slight difference between the two

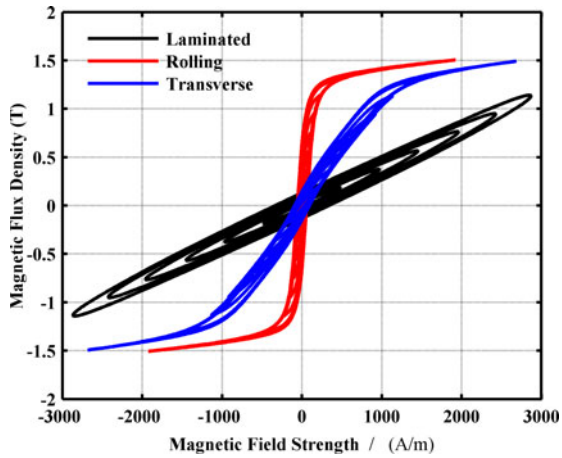


Fig. 15. Magnetic hysteresis loops of nonoriented silicon steel in three directions.

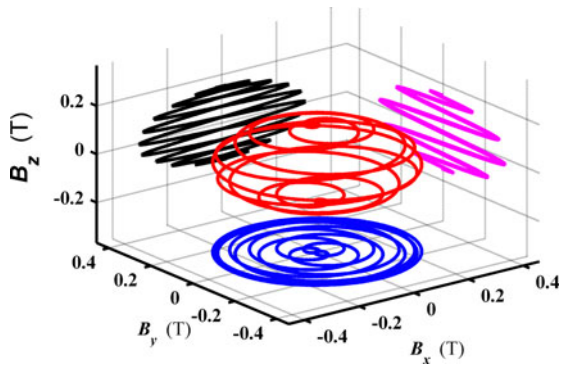


Fig. 16. $\boldsymbol{B}$ loci and corresponding projections of 3-D spherical excitation of 3-D magnetic properties measurement for nonoriented silicon steel sheet.

working states will cause a big error. However, the feedback and harmonic compensation method can guarantee that the difference of flux density between CW and CCW rotatiion is less than 0.3%. Therefore, the tensor effects is eliminaated in the rotational magnetization process.

C. Experiments of Alternating and 3-D Magnetization

The alternating magnetic hysteresis properties of the silicon steel lamination 35ww270 at 50 Hz are compared along the three directions as illustrated in Fig. 15. The magnetic permeability of silicon steel sheet along the rolling direction is larger than that along the transverse direction, which presents a strong magnetic anisotropy of nonoriented silicon steel sheet. Moreover, the permeability along the laminated direction is approximately linear, which is mainly determined by the stacking coefficient of the laminated silicon steel. The area of hysteresis loop represents the total loss of the tested specimen in one cycle. The alternating eddy currents and core losses in the direction normal to the lamination sheets is much larger than those of the other two directions.

Figs. 16 and 17 show the $\boldsymbol{B}$ and $\boldsymbol{H}$ loci of nonoriented silicon steel sheet under spherical magnetization. The purpose of

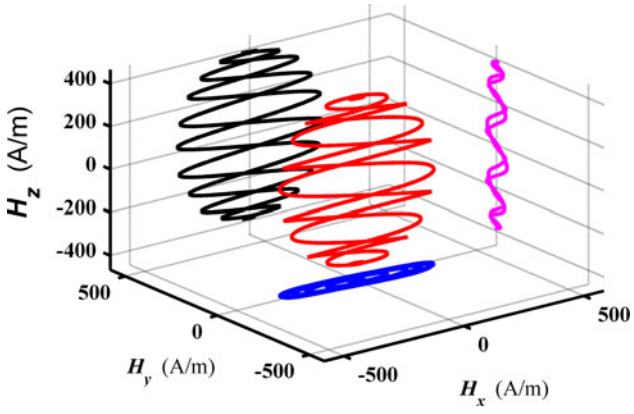


Fig. 17. $\boldsymbol{H}$ loci and corresponding projections of 3-D magnetic properties measurement for nonoriented silicon steel sheet.

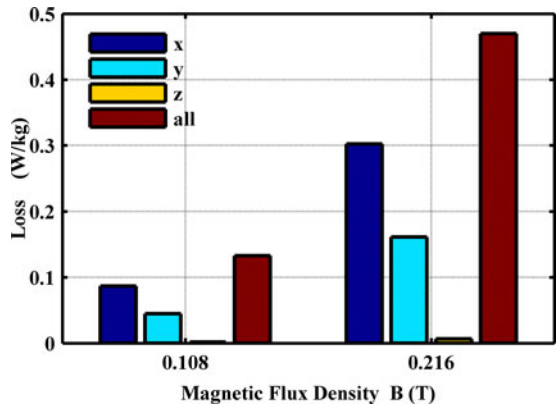


Fig. 18. Core loss feature in each axis under 3-D spherical excitation.

the spherical excitation model is to testify that the 3-D magnetization system can form an arbitrary and periodical $\boldsymbol{B}$ locus inside the specimen. In this model, the excitation frequency in the *x*-*o*-*y* plane is 100 Hz, and the excitation frequency in the direction normal to the lamination sheets is 10 Hz in order to avoid strong skin effects. The *B*–*H* signals in all directions are processed by numerical integration, waveform smooth, and balance. Then, a group of $\boldsymbol{B}$ and $\boldsymbol{H}$ loci in the 3-D space can be plotted. The *H* sensing coils in the *x*- and *y*-axes are affected by the magnetic flux in the *z*-axis. Because the frequency of interference component in the *x*- and *y*-axes is lower than the fundamental frequency, the interference signal can be eliminated by frequency decomposition. The projections in the *x*–*o*–*y* plane of $\boldsymbol{H}$ loci are elliptical, which shows the magnetic anisotropy. Therefore, the *x*-axis is the magnetically hard direction and the *y*-axis is the magnetically easy direction. Fig. 18 shows the core loss feature of this nonoriented silicon steel specimen in each axis under the 3-D spherical magnetization. The hysteresis loop in the *x*- or *y*-axis is a combination of hysteresis loops with different magnitudes, while the hysteresis loop in the *z*-axis is a single loop. As a result, the core loss of the *z*-axis is much lower than that of the *x*- and *y*-axes.

VI. Conclusion

Three-dimensional magnetic properties are recognized in electrical engineering as one of the key factors in design and performance optimization of electromagnetic devices. In this paper, a newly designed 3-D magnetic property testing system was developed. The feedback control method, harmonic compensation method, and 3-D magnetic sensing method were comprehensively studied.

The 3-D magnetic testing structure was simulated and validated. The mutual inductance between different axes and the proportion of linkage flux were analyzed. Consequently, the excitation model considering the mutual inductance and saturation was established and identified.

The digital control method in the frequency domain is more efficient than that in the time domain. The phases and magnitudes of $\boldsymbol{B}$ in the 3-D space were decomposed and well controlled independently. By using the novel control method, various complex rotational excitation models, such as 2-D circular rotational model and 3-D spherical model were applied on the magnetic property measurement of the silicon sheet steels.

A novel waveform compensation method was proposed to weaken efficiently the $\boldsymbol{B}$ harmonics induced by the magnetic saturation. As a result, the magnetic hysteresis and core loss experimental results are more reliable and repeatable by means of the complex control methods.

References

[1] G. Lei, T. Wang, Y. Guo, J. Zhu, and S. Wang, "System-level design optimization methods for electrical drive systems: Deterministic approach," *IEEE Trans. Ind. Electron.*, vol. 61, no. 12, pp. 6591–6602, Dec. 2014, doi:10.1109/TIE.2014.2321338.

[2] Z. Zhang, L. Yu, L. Sun, L. Qian, and X. Huang, "Iron loss analysis of doubly salient brushless DC generators," *IEEE Trans. Ind. Electron.*, vol. 62, no. 4, pp. 2156–2163, Apr. 2015, doi:10.1109/TIE.2014.2349875.

[3] Q. Yu, B. Bilgin, and A. Emadi, "Loss and efficiency analysis of switched reluctance machines using a new calculation method," *IEEE Trans. Ind. Electron.*, vol. 62, no. 5, pp. 3072–3080, May 2015, doi:10.1109/TIE.2015.2392716.

[4] E. Cardelli and A. Faba, "A benchmark problem of Vector magnetic hysteresis for numerical models," *IEEE Trans. Magn.*, vol. 50, no. 2, Feb. 2014, Art. no. 7026004, doi:10.1109/TMAG.2013.2282835.

[5] S. Zurek, "Qualitative analysis of Px and Py components of rotational power loss," *IEEE Trans. Magn.*, vol. 50, no. 4, Apr. 2014, Art. no. 6300914, doi:10.1109/TMAG.2013.2291225.

[6] H. Pfutzner, E. Mulsasalihovic, H. Yamaguchi, D. Sabic, G. Shilyashki, and F. Hofbauer, "Rotational magnetization in transformer cores—A review," *IEEE Trans. Magn.*, vol. 47, no. 11, pp. 4523–4533, Feb. 2008, doi:10.1109/TMAG.2011.2151201.

[7] R. Mazurek, H. Hamzehbahmani, A. J. Moses, P. I. Anderson, F. J. Anayi, and T. Belgrand, "Effect of artificial burrs on local power loss in a three phase transformer core," *IEEE Trans. Magn.*, vol. 48, no. 4, pp. 1653–1656, Apr. 2012, doi:10.1109/TMAG.2011.2173668.

[8] M. A. Jones and A. J. Moses, "Comparison of the localized power loss and flux distribution in the butt and lap and mitred overlap corner configurations," *IEEE Trans. Magn.*, vol. 10, no. 2, pp. 321–326, Jun. 1974, doi:10.1109/TMAG.1974.1058328.

[9] Y. Zhang, M. Cheng, and P. Pillay, "A novel hysteresis core loss model for magnetic laminations," *IEEE Trans. Energy Convers.*, vol. 26, no. 4, pp. 993–999, Dec. 2011, doi:10.1109/TEC.2011.2160866.

[10] D. Lin, P. Zhou, Q. M. Chen, N. Lambert, and Z. J. Cendes, "The effects of steel lamination core losses on 3D transient magnetic fields," *IEEE Trans. Magn.*, vol. 46, no. 8, pp. 3539–3542, Aug. 2010, doi:10.1109/TMAG.2010.2043509.

[11] Z. Cheng *et al.*, "Effect of excitation patterns on both iron loss and flux in solid and laminated steel configurations," *IEEE Trans. Magn.*, vol. 46, no. 8, pp. 3185–3188, Aug. 2010, doi:10.1109/TMAG.2010.2044765.
[12] F. Fiorillo, L. Dupre, C. Appino, and A. Rietto, "Comprehensive model of magnetization curve, hysteresis loops, and losses in any direction in grain oriented Fe-Si," *IEEE Trans. Magn.*, vol. 38, no. 3, pp. 1467–1476, May 2002, doi:10.1109/20.999119.
[13] Y. Li, Q. Yang, Y. Liu, Z. Zhao, C. Zhang, and D. Li, "A novel combined B-H sensing coil in three-dimensional magnetic properties testing system," *IEEE Trans. Appl. Supercond.*, vol. 24, no. 3, Jun. 2014, Art. no. 9000704, doi:10.1109/TASC.2013.2285281.
[14] A. Lee, L. Fu, C. Tsai, and Y. Lin, "Nonlinear adaptive speed and torque control of induction motors with unknown rotor resistance," *IEEE Trans. Ind. Electron.*, vol. 48, no. 2, pp. 391–402, Apr. 2001, doi:10.1109/41.915418.
[15] S. Mehta and J. Chiasson, "Nonlinear control of a series DC motor: Theory and experiment," *IEEE Trans. Ind. Electron.*, vol. 45, no. 1, pp. 134–142, Feb. 1998, doi:10.1109/ACC.1997.611799.
[16] M. Kuczmann, "Vector preisach hysteresis modeling: Measurement, identification and application," *Physica B*, vol. 46, no. 8, pp. 1403–1409, Apr. 2011, doi:10.1016/j.physb.2011.01.037.
[17] S. Zurek, P. Marketos, T Meydan, and A. J. Moses, "Use of novel adaptive digital feedback for magnetic measurements under controlled magnetizing conditions," *IEEE Trans. Magn.*, vol. 41, no. 11, pp. 4242–4249, Nov. 2005, doi:10.1109/TMAG.2005.854438.
[18] C. Ragusa and F. Fiorillo, "A three-phase single sheet tester with digital control of flux loci based on the contraction mapping principle," *J. Magn. Magn. Mater.*, vol. 304, no. 2, pp. e568–e570, Feb. 2006, doi:10.1016/j.jmmm.2006.02.177.
[19] O. Stupakov, "System for controllable magnetic measurement with direct determination," *J. Magn. Magn. Mater.*, vol. 324, no. 4, pp. 631–636, Feb. 2012, doi:10.1016/j.jmmm.2011.08.058.



Changgeng Zhang received the B.E. degree in electrical engineering from Tianjin Polytechnic University, Tianjin, China, in 2009, and the M.S. degree in computational mathematics from Nankai University, Tianjin, in 2012. He is currently working toward the Ph.D. degree at Hebei University of Technology, Tianjin, China.

His research interests include measurement magnetic properties and modeling of magnetic materials.



Yongjian Li (M'10) was born in Hebei, China, in 1978. He received the B.E., M.E., and Ph.D. degrees in electrical engineering from Hebei University of Technology, Tianjin, China, in 2002, 2007, and 2011, respectively.

From April 2009 to April 2011, he was a Visiting Research Fellow in the Center for Electrical Machines and Power Electronics, Faculty of Engineering, University of Technology Sydney, Sydney, Australia. He is currently a Professor in the School of Electrical Engineering, Hebei University of Technology. His research interests include measurement magnetic properties, modeling of magnetic materials, and power electronics.



Jingsong Li received the B.E. degree from Chengdu University of Technology, Chengdu, China, in 2010, and the M.E. degree from Tianjin Polytechnic Univeristy, Tianjin, China, in 2013, both in electrical engineering. He is currently working toward the Ph.D. degree at Hebei University of Technology, Tianjin, China.

His research interests include magnetic losses characteristics modeling and measurement analysis and application of magnetic materials in electrical engineering.



Qingxin Yang received the B.E., M.E., and Ph.D. degrees in electrical engineering from Hebei University of Technology, Tianjin, China, in 1983, 1986, and 1997, respectively.

He is the President of Tianjin Polytechnic University, Tianjin. His research interests include electromagnetic field computation and contactless power transfer.

Dr. Yang is a Board Member of the International COMPUMAG Society and the President of the China Electrotechnical Society.



Jianguo Zhu (S'93–M'96–SM'03) received the B.E. degree from Jiangsu Institute of Technology, Zhenjiang, China, in 1982, the M.E. degree from Shanghai University of Technology, Shanghai, China, in 1987, and the Ph.D. degree from the University of Technology Sydney (UTS), Sydney, Australia, in 1995, all in electrical engineering.

He is currently a Professor of electrical engineering and the Head of the School of Electrical, Mechanical and Mechatronic Systems, UTS. His current research interests include electromagnetics, magnetic properties of materials, and electrical machines.